NUMERICAL INVESTIGATION OF LOCAL HEATING EFFECT ON PARTICLE DEPOSITION IN AN EVAPORATING SESSILE DROPLET

Lounès Tadrist

Proceedings of the 17th International Heat Transfer Conference, IHTC-17
14 – 18 August 2023, Cape Town, South Africa

IHTC-17 | ID: 253

NUMERICAL INVESTIGATION OF LOCAL HEATING EFFECT ON PARTICLE DEPOSITION IN AN EVAPORATING SESSILE DROPLET

M. Ait Saada[1*], S. Chikh[1], L. Tadrist[2]

[1]USTHB, Faculté de Génie Mécanique et de Génie des Procédés, LTPMP, Alger 16111, Algérie
[2]Aix-Marseille Université, CNRS, Laboratoire IUSTI, UMR 7343, Marseille 13453, France

ABSTRACT

The effect of local heating on particle deposition in an evaporating colloidal sessile droplet is investigated numerically. A computer code is developed and implemented to simulate the coupled phenomena of flow and heat and mass transfer with phase change of the evaporation sessile droplet. The corresponding numerical model considers evaporative cooling effect, surface tension gradient effect at the liquid-air interface and buoyancy effect in the fluid phases. Results shows that particle deposit is controlled by the liquid motion inside the droplet. When the solid surface of substrate is subject to partly isothermal and adiabatic boundary conditions, multicellular flows with different orientations develop inside the droplet. With preponderant thermos-capillary effect, the particle concentration is pronounced at the drop center. An isothermal solid surface amplifies this effect whereas an adiabatic surface yields a more uniform particle concentration at the substrate surface.

KEY WORDS: Evaporation, sessile droplet, flow pattern, Interfaces, coupling heat and mass transfer, particle deposit

1. INTRODUCTION

Sessile droplet evaporation is a complex physical problem which involves fluid flow, heat and mass transfer as well as interactions between solid, liquid and gas phases throughout moving interfaces and a pinned or receding contact line. The formation of solid deposits during evaporation of colloidal sessile droplets arouses increasing interest because the control of size and shape of the deposits which are crucial for designing new applications as in inkjet printing, biosensors, nano-coatings, chip manufacturing and disease diagnostic techniques [1].

There are few numerical studies on particle deposition in the literature [2]. Overall, the experimental studies aim to identify the deposition patterns and trying to understand the mechanisms of their formation. Particle deposition is mainly influenced by the internal flow of the evaporating sessile drop; the effect of particle-substrate interaction is negligible [3]. Flow magnitude and pattern change depending on substrate thermal nature [4]. If the substrate is a good heat conducting, the internal flow is controlled by thermo-capillarity and the strong evaporation near the contact line. If it is good thermal insulating, the evaporation is highly reduced [7]. Deegan et al. [5] showed that outward radial flow due to the combined effect of pining contact line and high evaporation flux near the contact line, brings the particles towards the triple line forming a pattern in ring shape. Hu and Larson [6] demonstrated that in presence of the thermo-capillary effect due to evaporative cooling, a Marangoni flow cell grows inside the drop involving the formation of a central bump pattern. From these limiting cases where the colloidal drop evaporates on a homogeneous substrate of different natures, the understanding of the deposition mechanisms induced by the internal flow of the drop is fundamental for controlling size and shape of particle deposit at the end of the evaporation process.

*Corresponding Author: m_aitsaada@yahoo.fr

In the present work, we study numerically the evaporation of a colloidal sessile droplet. A comprehensive evaporation model is developed taking into account the thermo-capillary convection in both liquid and gas phases and buoyancy-induced convection in the surrounding air. Here, we focus on the analyze of the influence of local heating-induced flow pattern on particle transport within the droplet and deposition pattern forming at the end of evaporation. Local heating of the droplet is assumed by partly adiabatic and isotherm boundary conditions applied at the wetting solid surface of the substrate. Our study begins by presenting the mathematical model as well as the physical and computational domain. Next, a short presentation of the numerical procedure and validation is given. The last section is devoted to the results.

2. MATHEMATICAL MODEL

Figure (1) represents the physical domain of an axisymmetric sessile colloidal droplet with an initial volume of 10 mm^3. The droplet of dilute colloidal suspension evaporates on a very large horizontal hydrophilic solid surface (radius R_∞ = 50 R, initial contact angle θ_0 = 78°). The wetting solid surface on which the droplet evaporates, is subjected either to an isothermal boundary condition (heating wall temperature T_w = 26°C), an adiabatic boundary condition or a partially adiabatic and isothermal boundary condition. During evaporation, the contact line remains pinned and the droplet retains the shape of a spherical cap [7]. The ambient air temperature is $T_\infty = 25^\circ$ C and its relative humidity is Ha = 40%.

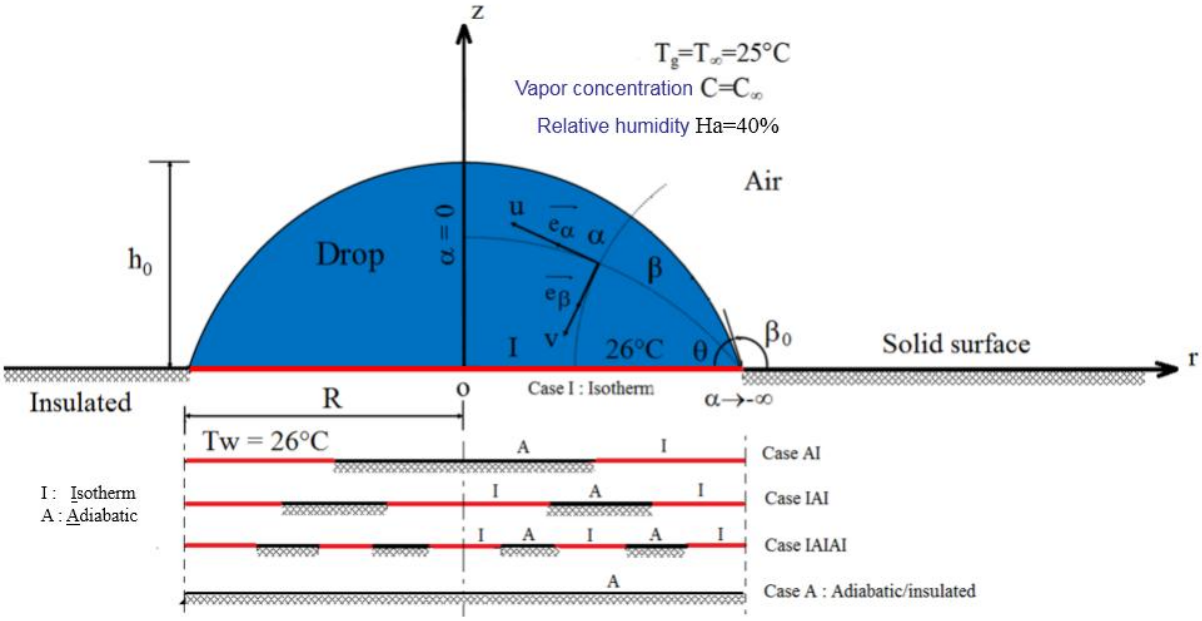

Fig. 1 Physical domain. The droplet is deposited on a solid surface with different boundary conditions.

The mathematical formulation of the problem is based on continuity equation (Eq.1), Navier-Stokes equations (Eq.1) and energy equation (Eq.3) in fluid phases as well as particle concentration equation in the droplet (Eq.4) and vapor concentration equation in surrounding air (Eq.5). The Boussinesq approximation is used to model the effect of thermal buoyancy in the liquid phase and the effect of thermo-solutal buoyancy in the gas phase. The effect of particle-substrate interactions on the deposition process is negligible compared to the effect of the internal flow of the droplet [3]. The thermo-physical properties of the dilute colloidal suspension are independent of the particle concentration [6]. The governing equations are written in toroidal coordinates to ensure better control of exchanges at the liquid-gas interface [4], they are given as follows:

$$\nabla \cdot U = 0 \tag{1}$$

$$\rho(U \cdot \nabla)U = -\nabla P + \mu \Delta U - \rho g \left[\beta_T (T - T_\infty) + \gamma \beta_C (C - C_\infty)\right] I \tag{2}$$

$$U \cdot \nabla T = \alpha_T \Delta T \tag{3}$$

$$U \cdot \nabla C = D \Delta C \tag{4}$$

$$\frac{\partial X_p}{\partial t} + \nabla . \left(\mathrm{U}\, X_p - D_p \nabla X_p \right) = 0 \tag{5}$$

In Eq. (2), I is a unit vector such as $\vec{I} = -\vec{e}_z$ and γ is equal to 1 in gas phase and 0 in liquid phase.

Solving the governing equations requires associated boundary conditions. Far from the droplet, the fluid is quiescent and the concentration of the vapor is given by $H_a\, C_v(T_\infty)$, where $C_v(T_\infty)$ is the saturation concentration at T_∞. On the solid surface, we have non-slip condition, no particle-solid interaction and no vapor permeability. Thermal boundary conditions are indicated in Fig. 1.

At the liquid-gas interface, the following conditions are set.

i) mass continuity

$$\rho_l \left(U_l - U_I \right) \cdot n = \rho_g \left(U_g - U_I \right) \cdot n = J \cdot n \tag{6}$$

$\vec{n}$ is a normal unit vector, $\vec{U}_I$ is the velocity of the moving interface and J is the local evaporation flux evaluated by:

$$J = J \cdot n = -D \nabla C \cdot n = -D \frac{\partial C}{h_\beta \, \partial \beta}\bigg|_{\beta_0} \tag{7}$$

h_β is the metric coefficient of the toroidal coordinate.

ii) mechanical stress balance

$$\left[\left(n \bar{\bar{\tau}} \right)_l - \left(n \bar{\bar{\tau}} \right)_g \right] \cdot t = \nabla \sigma \cdot t \tag{8}$$

$\vec{t}$ is a tangential unit vector and $\bar{\bar{\tau}}$ is the stress tensor. The surface tension gradient in the equation represents the term due to-the thermo-capillary effect.

iii) vapor concentration and thermal conditions

$$T_l = T_g \tag{9}$$

$$J\, h_{lg} - q_l \cdot n + q_g \cdot n = 0 \tag{10}$$

$\vec{q} = -k \vec{\nabla} T$ is the heat flux and $h_{\lambda g}$ is the latent heat of evaporation. Equation (9) expresses the thermal equilibrium and Eq.(10) the energy balance. Air at the interface is in a saturated state; its vapor concentration depends on temperature according to a polynomial relationship:

$$C_v(T) = \sum_{i=0}^{4} a_i T^i \tag{11}$$

The coefficients a_i are chosen to fit experimental data of Raznjevic [8]. The evaporation rate $\dot{M}$ over the whole drop surface is determined by:

$$M = -2\pi D \int_0^{-\infty} \frac{\partial C}{h_\beta \partial \beta}\bigg|_{\beta_0} h_\phi h_\alpha \, d\alpha \tag{12}$$

where h_α, h_β and h_ϕ are the metric coefficients of the toroidal coordinates α, β and ϕ, respectively.

iv) particle concentration condition

Particles do not cross liquid-gas interface, which is expressed by:

$$\left[-D_p \nabla X_p + (\mathrm{U} - \mathrm{U}_{int})\, X_p \right] . n = 0 \tag{13}$$

Particle concentration gradient is locally equal to zero at solid surface during evaporation time. Towards the end of droplet life, the motionless particles settle vertically on the solid surface. Resulting distribution of particle surface concentration (mass density) gives the final profile of the deposit.

3. NUMERICAL PROCEDURE

The governing equations (1-5) with the corresponding boundary and interface conditions are solved by means of the finite volume method [9]. Staggered grids are utilized in fluid phases with a very fine cell size (order of 10^{-5} R) around the contact line. The velocity-pressure coupling is handled using the SIMPLE algorithm. The PLDS Scheme is adopted to discretize convection and diffusion terms in governing equations. The solution method of the system of algebraic equations is based on a combination of Thomas Algorithm and the Gauss-Seidel point iterative method. Several convergence criteria of the iterative process are set. The solution is reached once the maximum relative error on each dependent variable is less than 0.1%, the maximum residue of each conservation equation is less than 10^{-5} and the maximum allowable residue of continuity equation is less than 10^{-10}.

The computation program elaborated is validated by comparison with the experimental data of Gleason et al. [10]. These authors conducted a series of experiments using infrared thermography and microscope imaging methods and showed the effect of substrate temperature on the evaporation kinetics of a sessile drop of water. Figure 2 shows a comparison of evaporation rate and specific evaporation rate results. Good agreement is found between the two approaches especially at wall temperatures below 55°C.

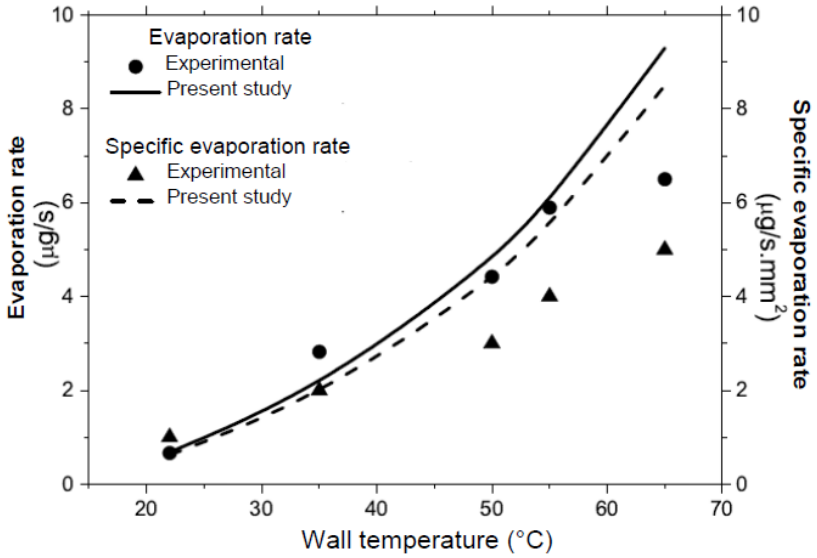

Fig. 2 : Evaporation rate versus wall temperature T_w. The obtained numerical results are compared with experimental results of Gleason et al [10] showing the wall temperature effect on the evaporation rate and specific evaporation rate of a water sessile drop at contact angle of 80.

4. RESULTS AND DISCUSSION

The aim of this study is to highlight the influence of the internal thermo-capillary flow on the transport and the particle deposition in an evaporating colloidal sessile droplet. The colloidal suspension of the droplet consists of polystyrene nanoparticles with 100 nm diameter diluted in water (initial concentration of 0.1 kg/mm^3, mass diffusion coefficient of 1.7×10^{-11} m^2/s). Five cases of thermal boundary conditions (BCs) are applied at the wetting solid surface of the substrate: case I (totally Isothermal), case A (totally Adiabatic), case AI (partially Adiabatic-Isothermal), case IAI (partially Isothermal-Adiabatic-Isothermal) and IAIAI case (partially Isothermal-Adiabatic-Isothermal-Adiabatic-Isothermal).

Velocity and temperature fields are presented in figure (3) for contact angles of 50° and 20°. At beginning of evaporation (θ = 50°), a counterclockwise unicellular flow appears in the droplet for all cases of BCs due to the Marangoni effect induced by the monotonic variation of the temperature along the liquid-gas interface. At contact angle of 20°, for cases I, A and AI, the flow remains counterclockwise unicellular pattern, while for the case IAI, it becomes bi-cellular pattern with an anticlockwise cell at droplet edge followed by a clockwise cell in droplet volume. For case IAIAI, the flow becomes quadri-cellular pattern shared between two zones. In the first zone at droplet edge, there is a 1st counterclockwise cell followed by a 2nd clockwise cell. In the second zone at droplet center, we have an anticlockwise cell followed by a clockwise cell. This is due to the locations of the isothermal and adiabatic sections at droplet base which generate four cells with successively opposite flow directions. For temperature fields in liquid phase, thermal convective effects become negligible at contact angles lower than 20°, especially for totally isothermal or adiabatic BCs.

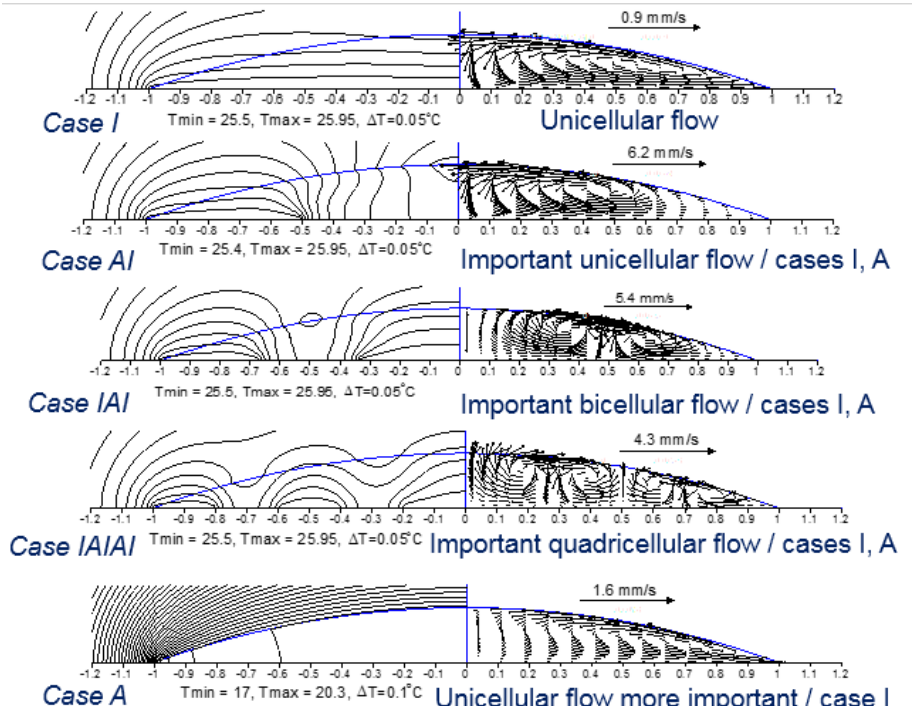

Fig. 3 : Isotherms (left) and velocity fields (right) for contact angle of 20°.

Figure (4) illustrates temperature profiles at droplet surface for contact angles of 50° and 20°. At contact angle of 50°, we notice an increasing temperature variation for the case of isothermal boundary condition (I), which corresponds to positive temperature gradients along the liquid-gas interface, explaining the presence of a single cell of counterclockwise flow within the droplet. The temperature difference between contact line and droplet top decreases in time and tends to zero towards the end of evaporation, implying Marangoni effect elimination. Passing to adiabatic BC case (A), the droplet is strongly cooled. The surface temperature always follows an increasing variation, but remains weak in a first phase followed by a strong increase approaching the contact line. For mixed thermal boundary conditions, the influence on the surface temperature is much greater at contact angles less than 20° compared to the isothermal BC (I). For this stage of evaporation, the temperature for case AI is strongly increasing at droplet center and weakly increasing at droplet edge. For other remaining BCs cases (IAI and IAIAI), it follows a non-monotonic variation, involving positive or negative temperature gradients along the liquid-gas interface depending on isothermal or adiabatic section present below the droplet surface. The temperature in these cases is characterized by a strong decrease in presence of an adiabatic section and a weak increase in presence of an isothermal section. The change in direction of temperature gradients explains the presence of multicellular flow inside the droplet.

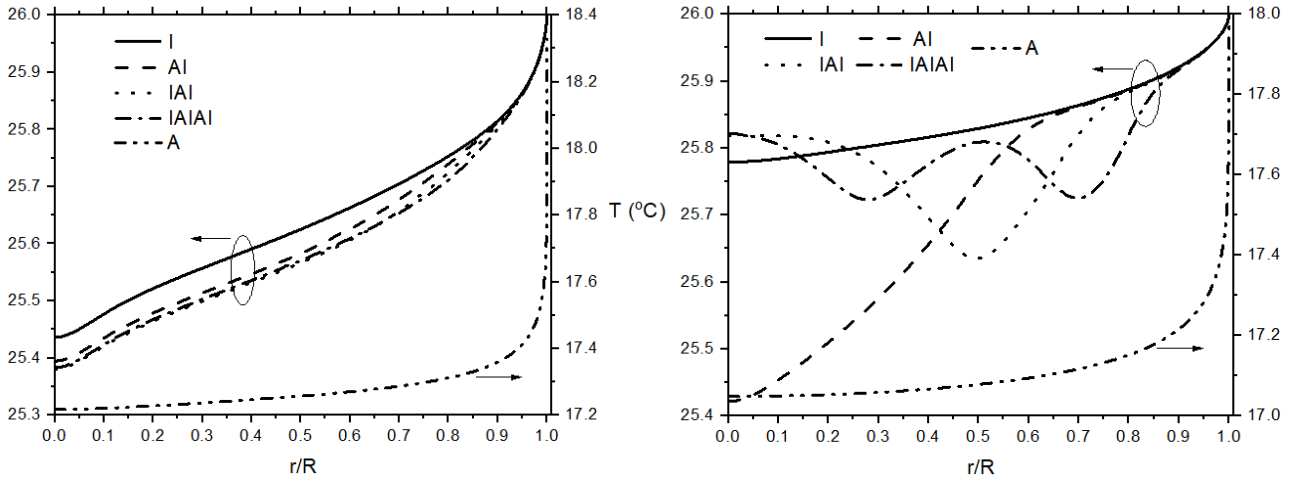

Fig. 4.. Temperature profiles at droplet surface for θ = 50° and 20°.

Particle concentration fields are plotted in figure (5) for contact angle of 5°. These mass fields which are influenced by flow patterns, differ from each other relatively to the five cases of thermal boundary conditions (I, AI, IAI, IAIAI, A). For isothermal case (I), a small particle concentration is noted at droplet edge while the concentration is higher in the central part of the droplet. For BCs cases A and AI, there is less concentration at droplet center which increases towards the contact line. For other cases (IAI and IAIAI), the multicellular flow induces a much high concentration in the zone near the contact line and a less high concentration towards the droplet axis.

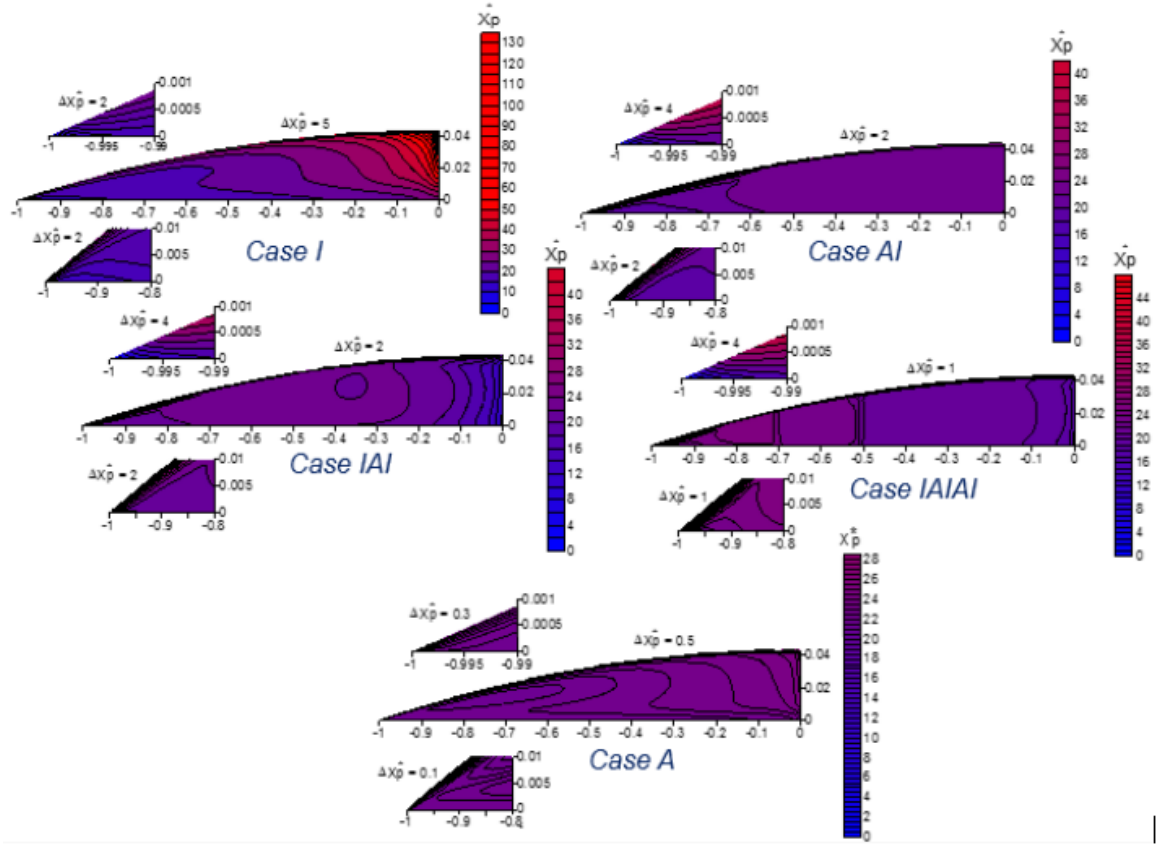

Fig. 5 Particle concentration fileds for the contact angle of 5°.

Figure 6 represents distributions of particle surface concentration at droplet base where different thermal boundary conditions are applied. Particle surface concentration $X_{p,s}$ is evaluated at the end of evaporation corresponding to a contact angle of 1°. Figure 6 (a) corresponds to variation of $X_{p,s}$ as a function of radial position (r/R). Figure 6 (b) corresponds to variation of $X_{p,s}$ as a function of dimensionless surface $(r/R)^2$ around droplet axis, it allows to verify particle mass conservation in the droplet during evaporation process. There is no interaction between particles and substrate. The particles are transported by the flow and they deposit vertically on the substrate at contact angle of 1°.

By analyzing Fig. 6 (a) for isothermal BC case (I), we note a maximum surface concentration around droplet axis which decreases until tending towards a zero value at the contact line. Here, we have a particle deposit in form of a central bump. For BCs cases A or AI, there is spreading of the central bump on droplet base, which is shown by a decrease in the variation of $X_{p,s}$ due to the importance of thermo-capillary flow in the zone close to the contact line. For other BCs cases (IAI and IAIAI), the multicellular flow induces an even more spread out particle deposition. There is a tendency of almost uniform distribution of particle surface concentration.

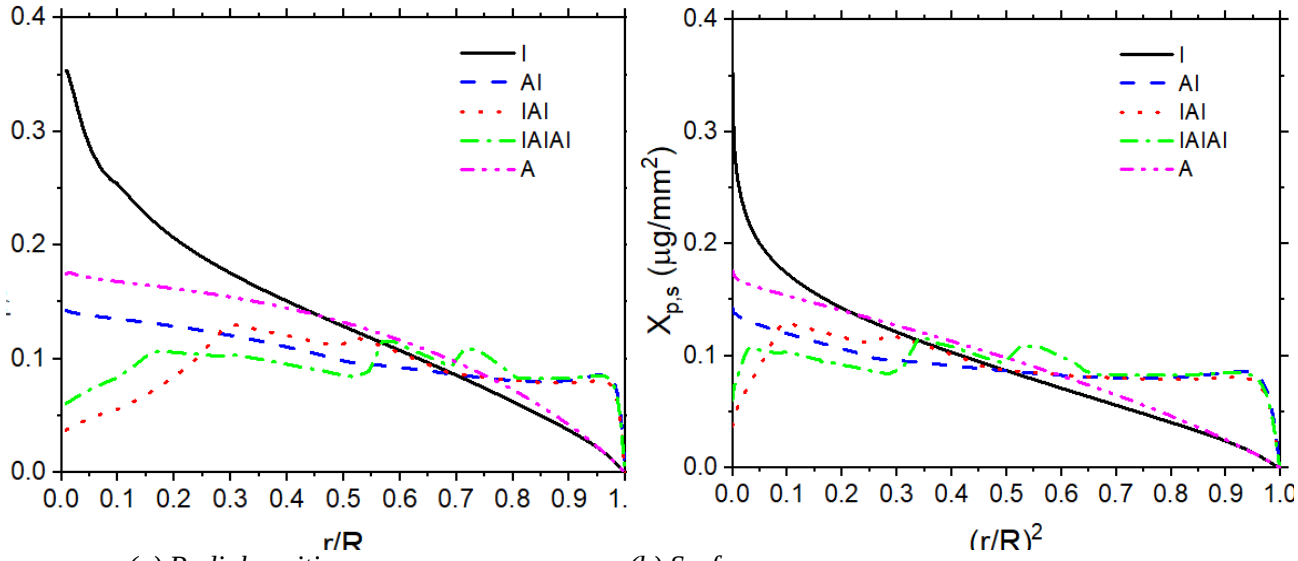

(a) Radial position *(b) Surface area*

Fig. 6 Distribution of particle surface concentration for different cases of thermal BCs (I, AI, IAI, IAIAI, A). (a) Dimensionless radial position, (b) Dimensionless surface area.

5. CONCLUSION

A numerical study of particle deposition is carried out by considering the evaporation of a colloidal droplet on a locally heated solid surface. Isothermal and adiabatic sections are arranged alternately at the base of the droplet for materializing the thermal heterogeneity of the solid surface. A numerical model is developed taking into account the effects of evaporative cooling, thermo-capillarity and thermal or thermo-solutal buoyancy. The obtained results highlighted the existence of multicellular flows of different orientations developing inside the droplet. Applying a totally isotherm boundary condition induces a higher particle concentration at droplet center (bump-like deposit) while the totally adiabatic (or partly adiabatic and isotherm) boundary condition induces spreading of particle concentration towards the droplet edge. The presence of multicellular flow gives an almost uniform particle concentration on the substrate at the end of evaporation. The preponderant radial motion induces a more important particle concentration at the droplet periphery (case widely discussed in the literature).

NOMENCLATURE

C	concentration	(kg/m^3)
C_v	saturated vapor concentration	(kg/m^3)
D	vapor diffusion coefficient	(m^2/s)
D_p	particle diffusion coefficient	(m^2/s)
$h_{\lambda g}$	latent heat of vaporization	(J/kg)
H_a	relative humidity	(-)
k	thermal conductivity	(W/m K)
J	evaporation flux	(kg/m^2 s)
$\dot{M}$	evaporation rate	(kg/s)
R	contact radius	(m)
r, z	cylindrical coordinates	(m)
T	temperature	(°C)
t	time	(s)
$\vec{U}$	velocity vector	(m/s)
X_p	Particle concentration	(kg/m^3)

Greek Symbols

α, β, ϕ	toroidal coordinates	(rd)
α_T	thermal diffusivity	(m^2/s)
ρ	density	(kg/m^3)
μ	dynamic viscosity	(kg/m s)
θ	contact angle	(°)

Subscripts

l, g	liquid, gas
∞	at infinity in surrounding air

REFERENCES

[1] Zanga, D., Tarafdar, S., Tarasevich, Y. Yu., Choudhury, M. D., and Dutta, T., ''Evaporation of a Droplet: From physics to application'', *Physics Reports*, Vol. 809, pp.1-56, (2019).

[2] Ait Saada, M., Chikh, S., Tadrist, L., ''A numerical study of particle transport in an evaporating colloidal sessile droplet'', *Interfacial Phenomena and Heat Transfer*, 4(4), pp.217–233, (2016).

[3] Bridonneau, N., Zhao, M., Battaglini, N., Mattana,, G., Thévenet V., Noël, V., Roché, M., Zrig, S., and Carn, F., ''Self-Assembly of Nanoparticles from Evaporating Sessile Droplets: Fresh Look into the Role of Particle/Substrate Interaction'' *Langmuir*, 36, 39, 11411–11421, (2020).

[4] Bouchenna, C., Ait Saada, M., Chikh, S., Tadrist, L., ''Generalized formulation for evaporation rate and flow pattern prediction inside an evaporating pinned sessile drop'', *International Journal of Heat and Mass Transfer*, Vol 109, pp. 482-500, (2017).

[5] Deegan, R. D., Bakajin, O., Dupont, T. F., Huber, G., Nagel, S. R., and Witten, T. A., ''Contact line deposits in an evaporating drop'', *The American Physical Society*, Vol 62, pp.756-765, (2000).

[6] Hu, H., and Larson, R. G., ''Marangoni Effect Reverses Coffee-Ring Depositions'', *J. Phys. Chem. B*, Vol 110, pp. 7090–7094, (2006).

[7] Ait Saada, M., Chikh, S., Tadrist, L., ''Evaporation of a sessile drop with pinned or receding contact line on a substrate with different thermophysical properties'', *International Journal of Heat and Mass Transfer*, Vol 58, pp. 197–208, (2013).

[8] Raznjevic, K., ''Handbook of thermodynamic tables'', Begell House, (1995).

[9] Patankar, S.V., ''Numerical heat transfer and fluid flow'', McGrawHill, Hemisphere, Washington, D.C, (1980).

[10] Gleason, K., Voota, H., and Putnam, S. A., Steady-state droplet evaporation: Contact angle influence on the evaporation efficiency. Int. J. Heat Mass Transfer (101) 418-426, (2016).